2020 IEEE Conference on Control Technology and Applications (CCTA)
August 24-26, 2020. Montréal, Canada

Continuously Differentiable Stick-Slip Friction Model with Applications to Cable Simulation Using Nonlinear Finite Elements

Cassidy Westin[1] and Rishad A. Irani[1]

Abstract— **This paper presents a continuously differentiable friction model based on the Quinn regularization of the Coulomb model in order to improve numerical performance for simulating dynamic systems using implicit ODE solvers. The implementation of the friction model for simulations of cable-pulley and cable-winch contact is demonstrated using the nonlinear Absolute Nodal Coordinate Formulation. Frictional contact between the cable and a dynamic surface is implemented using a Lagrange multiplier formulation. Examples of simple a capstan and a motorized pulley system are provided to demonstrate the stick-slip behavior of the model and the performance improvement over the original Quinn model, respectively. Using the ODE solver *ode15s*, the computation time was reduced by factors of 4.5 to 18.8 depending on the model parameters. The proposed model can be used to model and verify the behavior of dynamics systems in control applications.**

I. Introduction

Accurate simulation of mechanical systems often requires incorporating the dissipative and sticking effects due to friction. Implementing friction in numerical simulations can be difficult due to its discontinuity at zero velocity. Many approaches for modeling friction have been developed including continuous velocity-dependent models such as the Dahl [1] and LuGre [2] models, which are simple to implement in simulations but do not capture the sticking behavior. Elastic or bristle friction models permit an elastic pre-sliding displacement in the sticking phase [3], however they tend to be inefficient due to their complexity and oscillatory behavior [4]. Regularizations of the classical Coulomb friction model have been developed by Karnopp [5] and Quinn [6] in order to balance accuracy and numerical performance, while also preserving the desired sticking behavior.

In particular, Quinn [6] proposed a continuous regularization of the Coulomb model to eliminate chattering behavior exhibited by discontinuous models such as the Karnopp model [5]. However, due to fact that the model is not continuously differentiable, one may encounter poor numerical performance using implicit ODE solvers which require the computation of the Jacobian of the external forces. Thus, a contribution of this work is a modified model, referred to as the Continuously Differentiable Quinn (CDQ) model, which ensures differentiability of the friction force over the entire domain.

The proposed model can be used in place of the Quinn model and other Coulomb regularizations to simulate the behavior of dynamic systems which exhibit stick-slip behavior such as robot joints, actuators and clutches. Simulations could then be used to develop and tune control algorithms in order to avoid undesirable behavior. Additionally, the friction model may be suitable for nonlinear model-based control methods such as Internal Model Control in which smoothness of the dynamic model is required [7].

One potential application is for simulating the cable-surface interactions in winch and pulley systems. The friction model can be used to simulate dynamics variations in the cable strain and contact forces. A simulation of these behaviors can then inform the development of control algorithms in order to mitigate undesirable behavior such as "bird-caging" due to detachment of the cable from the winch surface. The model can also be used to improve towed and vertical Active Heave Compensation systems [8], [9].

The authors previously developed a simulation [10] - [12] of cable-pulley and cable-winch systems utilizing the Absolute Nodal Coordinate Formulation (ANCF) to model the cable dynamics. The previous model did not include tangential friction, thus the second contribution of this work is an implementation of stick-slip friction between the cable and winch surface for ANCF cable elements. The proposed approach utilizes Lagrange multipliers to determine the magnitude of the force required to enforce the desired stiction behavior.

The next section contains a description of the Coulomb model of friction along with the Karnopp, Quinn and CDQ regularizations. Section III describes the ANCF cable model and the implementation of the friction force. In Section IV, simulations are performed to examine the model behaviors for simple systems and the computational performance of each friction model are compared. The paper ends with concluding remarks in Section V.

II. Friction Modelling

The classical model of friction or the Coulomb model comprises two cases, sliding and sticking. In the sliding case, the relative velocity v between the two surfaces is non-zero and the friction force F_f is

$$F_f = -\mu F_N \text{sgn}(v), \tag{1}$$

where μ is the friction coefficient and F_N is the normal force. In the sticking state, the relative velocity is equal to zero and the friction force is

$$F_f = -\min(\mu F_N, |F_{eq}|)\text{sgn}(F_{eq}), \tag{2}$$

[1]Department of Mechanical and Aerospace Engineering, Carleton University, Ottawa, Canada; cassidy.westin@carleton.ca; rishad.irani@carleton.ca

978-1-7281-7140-1/20/$31.00 ©2020 IEEE

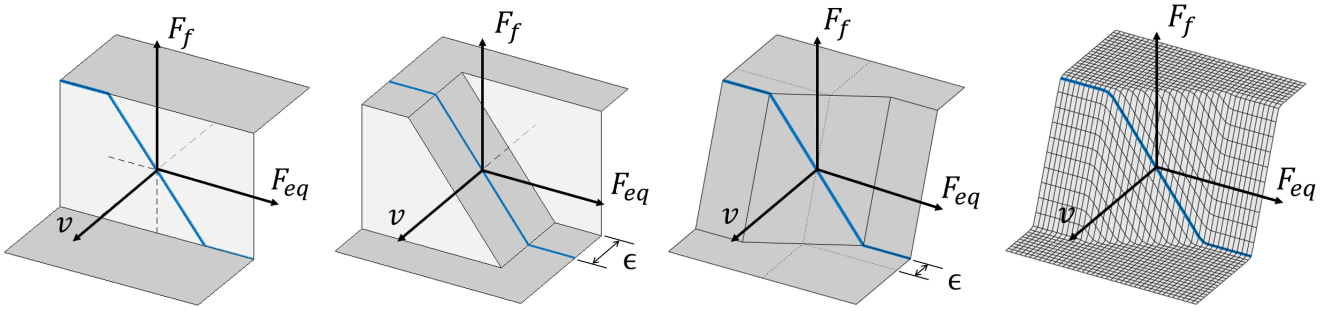

(a) Coulomb (b) Karnopp (c) Quinn (d) Continuously Differentiable Quinn (proposed)

Fig. 1: Surface plots of (a) Coulomb model, (b) Karnopp model, (c) Quinn model, and (d) proposed Continuously Differentiable Quinn model with $\alpha = 0.9$ and $\beta = 1.1$. The curve at $v = 0$ is shown as a solid blue line.

where F_{eq} is the sum of all other forces acting on the body in the direction tangential to the surface. Fig. 1a illustrates the Coulomb friction model and the relationship between F_f, F_{eq} and v. The blue line represents the friction force curve at zero velocity from (2). At a non-zero velocity the friction force is independent of the applied forces F_{eq} and has a constant magnitude, depending only on the direction of the sliding velocity v.

In a dynamic simulation, the sliding velocity v will not reach an exact value of zero due to limited numerical precision, thus implementations of stick-slip friction typically utilize a regularization of the Coulomb model, such as the Karnopp model [5]. Using the same axes as before, Fig. 1b illustrates the Karnopp friction model where a finite region $-\epsilon \leq v \leq \epsilon$ is defined in which the velocity is treated as having a value of zero. Thus, the friction force is defined

$$F_f = \begin{cases} -F_{eq}, & \text{if } |v| \leq \epsilon \\ -\mu F_N \text{sgn}(v), & \text{otherwise.} \end{cases} \tag{3}$$

The numerical solution of dynamics problems utilizing the Karnopp friction law can be difficult due to the discontinuity of the model at $|v| = \epsilon$ resulting in chattering, or repeated transitions between sticking and slipping states. In order to address this shortcoming of the Karnopp model, various continuous definitions of the friction force have been developed.

To eliminate the discontinuity in the Karnopp model, Quinn [6] proposed a new regularization of the Coulomb friction model which has the form

$$F_f = \begin{cases} -\dfrac{\mu F_N \bar{v}}{\epsilon}, & \text{if } |\bar{v}| \leq \epsilon \\ -\mu F_N \text{sgn}(\bar{v}), & \text{if } |\bar{v}| > \epsilon \end{cases} \tag{4}$$

where

$$\bar{v} = \begin{cases} v + \dfrac{\epsilon F_{eq}}{\mu F_N}, & \text{if } |F_{eq}| \leq \mu N \\ v + \epsilon \text{sgn}(F_{eq}), & \text{if } |F_{eq}| > \mu N. \end{cases} \tag{5}$$

Fig. 1c illustrates the Quinn model along the v, F_{eq} and F_f axes. The discontinuities of the Karnopp model are removed, while the behavior of the Coulomb model at zero velocity, represented by the solid blue line, is preserved exactly. A shortcoming of Quinn's model is that it is not continuously differentiable, due to the piece-wise definitions of the friction force F_f and velocity parameter $\bar{v}$. The slope discontinuities can make numerical solution of the equations of motion difficult when using implicit time-stepping algorithms, such as MATLAB's ODE suite [13], as the Jacobian of the external forces may become undefined due to the slope discontinuity. Thus, a modifications to Quinn's model is proposed in the following section in order to ensure the friction force is continuously differentiable in the entire domain.

A. Proposed Regularization

Equivalent to the form of the Quinn friction model in equation (4), a proposed alternate form is written as

$$F_f = -\mu F_N h(\bar{v}/\epsilon), \tag{6}$$

where $h(\bar{v}/\epsilon)$ is a piece-wise linear sigmoid function given by

$$h(x) = \begin{cases} x, & \text{if } |x| \leq 1 \\ \text{sgn}(x), & \text{otherwise.} \end{cases} \tag{7}$$

Using equation (7), the equation for the modified velocity $\bar{v}$ can also be written

$$\bar{v} = v + \epsilon h(F_{eq}/\mu F_N). \tag{8}$$

In order to make a continuously differentiable friction model, a modification to the Quinn model is proposed by replacing the piece-wise linear sigmoid function $h(x)$ with a smooth sigmoid function defined

$$h(x) = \begin{cases} x, & \text{if } |x| \leq \alpha \\ p_1(x), & \text{if } \alpha < x < \beta \\ p_2(x), & \text{if } -\alpha > x > -\beta \\ \text{sgn}(x), & \text{if } |x| \geq \beta \end{cases} \tag{9}$$

where α and β are parameters which define the boundaries of the linear and nonlinear regions and $p_1(x)$ and $p_2(x)$ are

cubic polynomial functions satisfying $p_1(\alpha) = -p_2(-\alpha) = \alpha$, $p_1(\beta) = -p_2(-\beta) = 1$, $p_1'(\alpha) = p_2'(-\alpha) = 1$, and $p_1'(\beta) = p_2'(-\beta) = 0$. Fig. 2 illustrates the proposed sigmoid function along with the piece-wise linear function used in Quinn's model along with the boundaries of the piece-wise segments.

In the region $-\alpha \leq x \leq \alpha$, the proposed sigmoid function is identical to the original piece-wise function. Thus, the sticking behavior of the Coulomb friction model, where the friction force exactly opposes the externally applied forces, is preserved in the region $|F_{eq}|/\mu F_N < \alpha$. Furthermore, in the limit as $\alpha \to 1$ and $\beta \to 1$, the proposed model converges to the original Quinn model. Fig. 1d illustrates the proposed friction model with $\alpha = 0.9$ and $\beta = 1.1$. Note that at zero velocity, the friction force saturates at a velocity smaller than the Coulomb force magnitude. As the system begins to slip and the sliding velocity increases the force quickly converges to the desired magnitude.

To examine the behavior of the proposed friction model and demonstrate its potential applications, the Quinn and CDQ friction models are implemented in a previously developed simulation of a flexible cable using nonlinear ANCF finite elements.

III. ANCF Cable Model

The cable model used to examine the proposed friction model utilizes the Absolute Nodal Coordinate Formulation [14] with each element comprising two nodes. Fig. 3 illustrates the ANCF element where the shape of the element is defined as a function of the parameter $p \in [0, L]$ by a cubic Hermite spline. Four vectors make up the element degrees of freedom: the Cartesian (absolute) position of each node $\mathbf{r}(0)$ and $\mathbf{r}(L)$ and a slope vector tangent to the cable centerline at each node $\mathbf{r}_p(0)$ and $\mathbf{r}_p(L)$, where $\mathbf{r}_p = \partial\mathbf{r}/\partial p$. The coordinates of an internal point on the element can be obtained by interpolating between the nodal coordinates using a cubic shape function matrix $\mathbf{S}(p)$,

$$\mathbf{r}(p) = \mathbf{S}(p)\mathbf{q} = [x \quad y \quad z]^T. \tag{10}$$

where L is the unstretched cable length, $\mathbf{q}$ is the vector of generalized coordinates given by

$$\mathbf{q} = \begin{bmatrix} \mathbf{r}(0)^T & \mathbf{r}_p(0)^T & \mathbf{r}(L)^T & \mathbf{r}_p(L)^T \end{bmatrix}^T \tag{11}$$

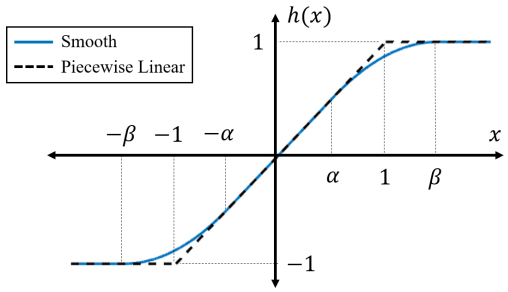

Fig. 2: Smooth sigmoid function (solid) and piece-wise linear sigmoid function (dashed)

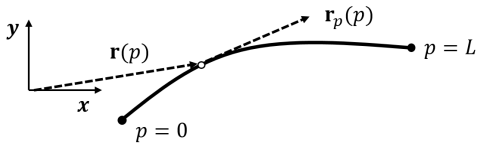

Fig. 3: Illustration of a planar ANCF element.

and the shape function $\mathbf{S}(p)$ is

$$\mathbf{S}(p) = \begin{bmatrix} \left(1 - 3\xi^2 + 2\xi^3\right)\mathbf{I} \\ \left(\xi - 2\xi^2 + \xi^3\right)\mathbf{I} \\ \left(3\xi^2 - 2\xi^3\right)\mathbf{I} \\ \left(-\xi^2 + \xi^3\right)\mathbf{I} \end{bmatrix}^T. \tag{12}$$

where $\xi = p/L$ is the arc parameter normalized by the element length and $\mathbf{I}$ is an identity matrix.

The generalized Newton-Euler equations are given for a single element as

$$\mathbf{M}\ddot{\mathbf{q}} + \mathbf{Q}_{\text{int}} - \mathbf{Q}_{\text{ext}} - \mathbf{Q}_c = 0, \tag{13}$$

where $\mathbf{M}$ is the mass matrix, $\mathbf{Q}_{\text{int}}$ is a generalized internal force vector, $\mathbf{Q}_{\text{ext}}$ is a generalized external force vector and $\mathbf{Q}_c$ is a constraint force. The internal force comprises the axial and transverse elastic forces and a damping force. The external force is the sum of the gravitational self-weight and the normal contact force. The constraint force will be used to enforce the stiction behavior of the surface contact. The definitions of each force is described in the following section.

A. Mass Matrix and Internal Forces

Using a variational mass lumping approach the mass matrix $\mathbf{M}$ is derived directly from the element kinetic energy [14] and is given by

$$\mathbf{M} = \frac{\partial^2 K}{\partial\dot{\mathbf{q}}\partial\dot{\mathbf{q}}} = \int_0^L \rho A \mathbf{S}(\mathbf{p})^T \mathbf{S}(\mathbf{p}) dp, \tag{14}$$

where K is the kinetic energy of the element, ρ is the cable density and A is the cable cross-sectional area.

Similarly, the elastic forces $\mathbf{Q}_e$ are derived from the strain energy U of the element [15] and are given by

$$\mathbf{Q}_e = \frac{\partial U}{\partial \mathbf{q}} = \int_0^L \left[EA\varepsilon \frac{\partial \varepsilon}{\partial \mathbf{q}} + EI\kappa \frac{\partial \kappa}{\partial \mathbf{q}} \right] dp, \tag{15}$$

where E is the Young's modulus of the cable material, A is the cross-sectional area, I is the second moment of area, ε is the longitudinal strain, and κ is the curvature of the element. The element curvature can be approximated by [15]

$$\kappa \approx |\mathbf{r}_{pp}|. \tag{16}$$

For the longitudinal strain ε, Berzeri and Shabana [15] suggest the Green-Lagrange strain defined as

$$\varepsilon = \frac{1}{2}\left[\left(\frac{\partial r}{\partial p} \right)^2 - 1 \right] = \frac{1}{2}\left[(\mathbf{S}_p\mathbf{q})^T (\mathbf{S}_p\mathbf{q}) - 1 \right]. \tag{17}$$

The internal damping force $\mathbf{Q}_d$ serves to include internal energy dissipation as well as improve the numerical stability of the simulation. The damping force is based on a Rayleigh dissipation function R representing one-half of the power dissipated during the motion given by

$$R = 1/2 \int_0^L c(\dot{\mathbf{r}}_p \cdot \dot{\mathbf{r}}_p) dp, \tag{18}$$

where c is a damping parameter and $\dot{\mathbf{r}}_p$ is the rate of change of the slope vector. Thus, energy is dissipated when the cable undergoes bending or axial deformations. The damping force can be written as

$$\mathbf{Q}_d = \frac{\partial R}{\partial \dot{\mathbf{q}}} = c \int_0^L \mathbf{S}_p^T \mathbf{S}_p dp \, \dot{\mathbf{q}}. \tag{19}$$

The integral in equation (15) is evaluated using a five point Guassian quadrature at each time step, whereas the integrals in equations (14) and (19) are constant and are evaluated symbolically at the start of the simulation.

B. External Forces

The external force vector $\mathbf{Q}_{ext}$ is the sum of the gravitational force $\mathbf{Q}_g$ and the normal contact force $\mathbf{Q}_N$.

The gravitational force is determined by integrating over the length of the element

$$\mathbf{Q}_g = \rho A \int_0^L \mathbf{S}^T \mathbf{g} dp, \tag{20}$$

where ρA is the mass per unit length and $\mathbf{g}$ is the gravity acceleration vector. As with the mass matrix, the gravitational force is constant and the integral is evaluated symbolically.

The normal contact force, in contrast, is concentrated at the first node of each element and is given by

$$\mathbf{Q}_N = \mathbf{S}(0)^T \mathbf{F}_N, \tag{21}$$

where $\mathbf{F}_N$ is a point force determined using a elastic penalty contact model. In the penalty method, the node is allowed to penetrate into the surface. The contact force is then defined as a function of the relative penetration δ. This work utilizes the Hunt-Crossley contact model [16] where the surface is represented as a nonlinear spring-damper and the contact force $\mathbf{F}_N$ is

$$\mathbf{F}_N = k_N \delta^n (1 + D\dot{\delta}) \mathbf{u}_N, \tag{22}$$

where $\mathbf{u}_N$ is the unit vector normal to the sheave surface at the point of contact, k_N is the contact stiffness, δ is the relative penetration of the node into the surface, D is a contact damping coefficient and n is a positive constant. For planar cable-winch or cable-pulley contact, the penetration δ is

$$\delta = \begin{cases} ||\mathbf{r} - \mathbf{r}_0|| - R, & \text{if } ||\mathbf{r} - \mathbf{r}_0|| < R \\ 0, & \text{otherwise,} \end{cases} \tag{23}$$

where R is the radius of the winch or pulley.

The magnitude of the contact force $F_N = ||\mathbf{F}_N||$ is used to determine the magnitude of the tangential friction force as described in Section II. The implementation of the tangential friction force in the ANCF model is described in the next section.

C. Friction Force

The friction forces are incorporated in the model in the form of an acceleration constraint using a method proposed by Udwadia and Kalaba [17] to calculate the magnitude of the constraint force. In the Udwadia-Kalaba method, a constraint of the form

$$\mathbf{A}(\mathbf{q}, \dot{\mathbf{q}}, t)\ddot{\mathbf{q}} = \mathbf{b}(\mathbf{q}, \dot{\mathbf{q}}, t) \tag{24}$$

is defined. The force $\mathbf{Q}_c$ applied to the system in order to satisfy the acceleration constraint is defined by introducing a vector of Lagrange multipliers λ such that

$$\mathbf{Q}_c = -\mathbf{A}^T \lambda. \tag{25}$$

The Lagrange multipliers are obtained by substituting $\ddot{\mathbf{q}} = \mathbf{A}^{-1}\mathbf{b}$ from equation (24) and the definition of the constraint force from equation (25) into equation (13). The Lagrange multipliers are thus

$$\lambda = \left[\mathbf{A}\mathbf{M}^{-1}\mathbf{A}^T\right]^{-1} (\mathbf{A}\mathbf{a} - \mathbf{b}), \tag{26}$$

where $\mathbf{a}$ is the associated accelerations of the unconstrained system,

$$\mathbf{a} = \mathbf{M}^{-1} (\mathbf{Q}_{ext} - \mathbf{Q}_{int}). \tag{27}$$

To implement the tangential friction using the Udwadia-Kalaba, the following acceleration constraint equation, which relates the axial acceleration of the node to the tangential surface acceleration, is proposed:

$$\mathbf{t}^T \mathbf{S}(0)\ddot{\mathbf{q}} - a_t = 0, \tag{28}$$

where $\mathbf{S}(0)\ddot{\mathbf{q}}$ is the acceleration of the node, $\mathbf{t}$ is the unit tangent vector aligned with the cable's longitudinal axis, and a_t is the tangential acceleration of the surface at the contact point. The constraint can be put directly in the form of equation (24) with $\mathbf{A} = \mathbf{t}^T\mathbf{S}(0)$ and $\mathbf{b} = a_t$.

Once the vector of Lagrange multipliers is obtained, they are modified according to the friction models described in Section II in order to allow for the sliding behavior. Since the Lagrange multiplier represents the magnitude of the force in violation of the constraint, it can be substituted for the external force F_{eq}. The normal force F_N is obtained from the magnitude of the penalty force determined by equation (22). Finally, the magnitude of the friction force F_f calculated from equation (6), is then substituted for $-\lambda$ in equation (25).

For a cable-winch system, the surface acceleration is given by

$$a_t = \dot{\omega} R, \tag{29}$$

where ω is the rotational velocity of the winch and R is the winch radius. The sliding velocity v is determined from

$$v = \mathbf{t}^T \mathbf{S}(0)\dot{\mathbf{q}} - \omega R. \tag{30}$$

In this work, the winch acceleration $\dot{\omega}$ is determined from a desired time-varying setpoint $\theta_d(t)$ using a PD control law,

$$\dot{\omega} = k_p(\theta_d - \theta) + k_d(\omega_d - \omega), \tag{31}$$

where k_p and k_d are constant gains and θ is the angular position of the winch, measured from the vertical axis. In the following section, simple cable-winch systems are simulated to examine the behavior of the friction implementation.

IV. Simulations and Results

To demonstrate the behavior and performance of the ANCF implementation and to compare the proposed friction model with the Quinn model, two scenarios are examined. First, a fixed drum or capstan with forces applied to the cable ends is simulated to demonstrate the stick-slip behavior of the friction model. Second, a rotating pulley is simulated and the computational performance of the proposed model is compared with the Quinn model. The simulations are performed in MATLAB. The ODE solver used for the simulations is the implicit, adaptive solver *ode15s*.

The cable parameters used for this analysis were taken from previous work [10] and are listed in Table I.

TABLE I: Simulation parameters.

Parameter	Value
Winch radius, R	0.25 m
Contact penalty, k_N	5×10^6 N/m
Contact damping parameter, D	1 Ns/m
Contact exponent, n	1.5
Coefficient of friction, μ	0.25
Friction regularization coefficient, ϵ	0.01 m/s
Cable longitudinal stiffness, EA	9.2×10^6 N
Cable cable bending stiffness, EI	0.7 Nm^2
Cable density, ρ	5.8×10^{-3} kg/m^3
Cable diameter, d	0.01 m

Scenario I: Capstan (Static Surface)

In the first scenario, the winch is fixed with disparate loads applied to the two ends of the cable. The winch thus functions as a capstan, where the friction serves to resist the load applied to one end of the cable. Fig. 4a illustrates the system consisting of a cylindrical drum supporting a cable with loads F_1 and F_2 applied to the two cable ends. The capstan equation gives the ratio between the load F_2 and the holding force F_1 at the point of slipping

$$F_2/F_1 = e^{\mu\phi}, \tag{32}$$

where μ is the coefficient of friction and ϕ is the wrap angle of the cable around the drum. For the system shown in Fig. 4a, the wrap angle has a nominal value of $\phi = \pi$. With a coefficient of friction of $\mu = 0.25$, the maximum ratio before slipping occurs is thus 2.19.

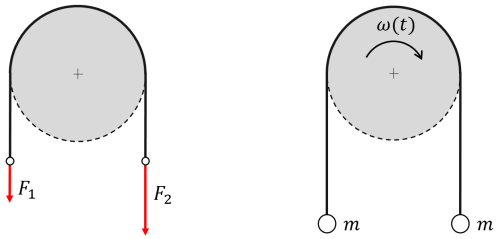

(a) (b)

Fig. 4: Diagram of (a) capstan system and (b) motorized pulley system.

In order to demonstrate the ability of the friction implementation to capture the desired stick-slip behavior, tests are performed by fixing the holding force F_1 and varying the loading force F_2, until the cable begins to slip. For these tests, the holding force F_1 was set at 98.1 N. Forty elements were used for the simulations. For the CDQ friction model, the friction parameters α and β were selected such that $\beta = 2 - \alpha$. Simulations were performed with α values of 0.5, 0.75, 0.9, 0.95 and 0.99.

Table II summarizes the results of the simulations under the Scenario I column. For the Quinn friction model, the cable began to slip at a force ratio of 2.24, while the proposed model slipped at ratios between 1.52 and 2.22. As expected, the proposed model sustains a lower amount of force, as the force saturates at a value smaller than the Coulomb force μF_N, whereas the Quinn model saturates at the Coulomb force. As the parameter α is increased and the CDQ model converges towards the Quinn model, the force ratio increases. It is also noteworthy that the Quinn model overestimates the slipping point. This error is likely due to nonlinearity in the normal contact force distribution that are not considered in the capstan equation. Fig. 5 shows the contact force distribution as a function of the contact angle of a 20, 40, and 60 element ANCF model and the linear assumption used in the capstan equation. The capstan equation considers only a linear distribution of the contact force, however in the ANCF simulation the contact force is nonlinear due to the bending stiffness and elastic definition of the normal forces. As the number of elements in the model increases, the amplitude of the variations diminishes, however the nonlinearity cannot be removed entirely. The ANCF model therefore will not exactly replicate the slipping behavior predicted by the capstan equation.

Scenario II: Motorized Pulley (Dynamic Surface)

The second scenario shown in Fig. 4b consists of a rotating pulley with a small mass attached to both ends of the cable. The desired rotation of the winch as a function of time $\theta_d(t)$ is selected to follow a cycloidal profile with amplitude $a = \pi/4$ and simulation time $\tau = 10$ s and can be written as

$$\omega(t) = \frac{t}{\tau} - \frac{a}{2\pi}\sin(2\pi t/\tau). \tag{33}$$

Fig. 6 shows the simulated displacement of one of the

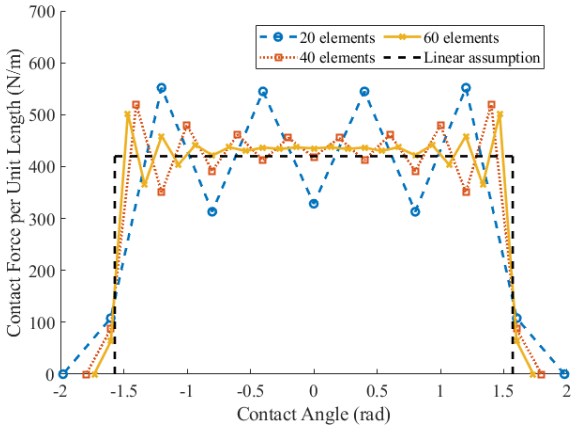

Fig. 5: Contact force distribution as a function of contact angle for the ANCF model with varying number of elements and linear model.

Model	Scenario 1	Scenario 2	
	Force Ratio	Comp. Time (s)	RMS Error (m)
Quinn	2.24	22804	–
CDQ ($\alpha = 0.99$)	2.22	5029	2.30×10^{-5}
CDQ ($\alpha = 0.95$)	2.16	1938	3.82×10^{-5}
CDQ ($\alpha = 0.90$)	2.08	1741	5.74×10^{-5}
CDQ ($\alpha = 0.75$)	1.80	1428	7.94×10^{-5}
CDQ ($\alpha = 0.50$)	1.52	1216	1.64×10^{-4}

TABLE II: Simulation results for Scenarios 1 and 2. RMS error for Scenario 2 is calculated relative to the Quinn friction model.

masses for the Quinn model and the CDQ model with $\alpha = 0.9$ as a function of time. Table II summarizes the results for the simulations in the Scenario II columns. The results obtained using the CDQ model are effectively identical to the Quinn model, with RMS errors ranging from 2.3×10^{-5} to 1.6×10^{-4} m; however, the Quinn model required a computation time of 22804 s using *ode15s*, while computation times for the proposed model ranged from only 1216 to 5029 s, an improvement by a factor of 4.5 to 18.8.

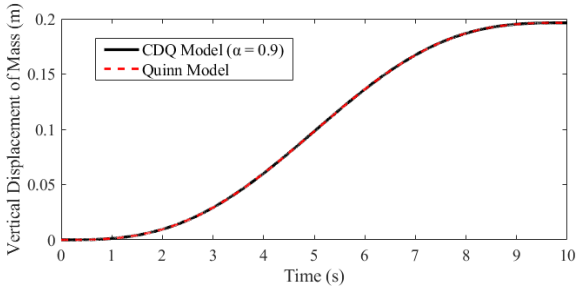

Fig. 6: Vertical displacement of load for motorized pulley simulation.

V. Conclusion

In this paper, a method was proposed for incorporating stick-slip friction models in simulations of cable-pulley and cable-winch interactions. In addition, a continuously differentiable regularization of the Coulomb friction model was proposed. The results of this study demonstrate the feasibility of the proposed approach. For a simple test case using the implicit ODE solver *ode15s*, the proposed model exhibited an improvement in the computation time over the standard Quinn model by a factor of at least 4.5 and up to a factor of 18.8. Future work will focus on implementing the friction model in a full scale simulation of a shipboard winch system [10]. Alternative ODE solvers may also be examined and implemented in order to improve the computational performance. Finally, the proposed model should be validated using experimental measurements for critical applications.

Acknowledgment

The authors would like to thank the Natural Sciences and Engineering Research Council of Canada (NSERC) and Carleton University for their support of this research.

References

[1] P. R. Dahl, "Solid friction damping of mechanical vibrations," *AIAA Journal*, vol. 14, no. 12, pp. 1675–1682, 1976.
[2] C. De Wit *et al.*, "A new model for control of systems with friction," *IEEE Trans. Automat. Contr.*, vol. 40, no. 3, pp. 419–425, 1995.
[3] D. A. Haessig Jr and B. Friedland, "On the modeling and simulation of friction," 1991.
[4] H. Olsson, K. J. Åström, C. C. De Wit, M. Gäfvert, and P. Lischinsky, "Friction models and friction compensation," *Eur. J. Control*, vol. 4, no. 3, pp. 176–195, 1998.
[5] D. Karnopp, "Computer simulation of stick-slip friction in mechanical dynamic systems," *J. Dyn. Syst., Meas., Control*, vol. 107, no. 1, pp. 100–103, 1985.
[6] D. D. Quinn, "A new regularization of Coulomb friction," *J. Vib. Acoust.*, vol. 126, no. 3, pp. 391–397, 2004.
[7] M. A. Henson and D. E. Seborg, "An internal model control strategy for nonlinear systems," *AIChE Journal*, vol. 37, no. 7, pp. 1065–1081, 1991.
[8] C. Calnan, R. J. Bauer, and R. A. Irani, "Reference-point algorithms for active motion compensation of towed bodies," *IEEE J. Oceanic Eng.*, vol. 44, no. 4, pp. 1024–1040, 2018.
[9] J. Woodacre, R. Bauer, and R. Irani, "Hydraulic valve-based active-heave compensation using a model-predictive controller with non-linear valve compensations," *Ocean Eng.*, vol. 152, pp. 47–56, 2018.
[10] C. Westin, "Modelling and simulation of marine cables with dynamic winch and sheave contact," Master's thesis, Carleton University, 2018.
[11] C. Westin and R. A. Irani, "Cable-pulley interaction with dynamic wrap angle using the absolute nodal coordinate formulation," in *Proc. 4th Int. Conf. of Contr., Dyn. Syst., and Robot. (CDSR'17)*, 2017.
[12] C. Westin and R. A. Irani, "Vortex-induced vibrations of a low-tension cable-sheave system modeled using nonlinear finite elements," in *Proc. 2018 CSME Int. Congr.*, pp. 1–6, Canadian Society of Mechanical Engineers, May 2018.
[13] L. F. Shampine and M. W. Reichelt, "The MATLAB ODE suite," *SIAM Journal on Scientific Computing*, vol. 18, no. 1, pp. 1–22, 1997.
[14] A. A. Shabana, "Flexible multibody dynamics: review of past and recent developments," *Multibody Sys. Dyn.*, vol. 1, no. 2, pp. 189–222, 1997.
[15] M. Berzeri and A. A. Shabana, "Development of simple models for the elastic forces in the absolute nodal co-ordinate formulation," *Journal of Sound and Vibration*, vol. 235, no. 4, pp. 539–565, 2000.
[16] K. Hunt and F. Crossley, "Coefficient of restitution interpreted as damping in vibroimpact," *J. Appl. Mech.*, vol. 42, no. 2, pp. 440–445, 1975.
[17] F. E. Udwadia and R. E. Kalaba, "A new perspective on constrained motion," *Proc. Roy. Soc. of London. Series A: Math. and Phys. Sci.*, vol. 439, no. 1906, pp. 407–410, 1992.